THE ASTROPHYSICAL JOURNAL, 488:781–791, 1997 October 20

INTERPRETATION OF THE CENTER-FILLED EMISSION FROM THE SUPERNOVA REMNANT W44

ILANA M. HARRUS,[1,2] JOHN P. HUGHES,[1,3] K. P. SINGH,[4] K. KOYAMA,[5] AND I. ASAOKA[6]
Received 1996 September 12; accepted 1997 May 29

ABSTRACT

We report the results of spectral and morphological studies of X-ray data from the supernova remnant (SNR) W44. Spectral analysis of archival data from the *Einstein Observatory*, *ROSAT*, and *Ginga*, covering a total energy range from 0.3 to 8 keV, indicates that the SNR can be described well by a nonequilibrium ionization (NEI) model with temperature ~ 0.9 keV and ionization timescale of order 6000 cm^{-3} yr. All elemental abundances are found to be within about a factor of 2 of their cosmic values, with iron possibly appearing to show significant depletion. No clear evidence for emission from supernova ejecta can be inferred from the observed metal abundances. The column density toward the SNR is high—around 10^{22} atoms cm^{-2}—as expected given the location of the remnant in the Galactic plane.

In addition to the spectral analysis, we have investigated two different evolutionary scenarios to explain the centrally brightened X-ray morphology of the remnant: (1) a model involving the slow thermal evaporation of clouds engulfed by the supernova blast wave as it propagates though a clumpy interstellar medium (ISM), and (2) a hydrodynamical simulation of a blast wave propagating through a homogeneous ISM, including the effects of radiative cooling. Both models can have their respective parameters tuned to reproduce approximately the morphology of the SNR. The mean temperature of the hot plasma in W44 as determined by our NEI X-ray analysis provides the essential key to discriminating between these scenarios. Based on the size (using the well-established distance of 3 kpc) and temperature of W44, the dynamical evolution predicted by the White & Long model gives an age for the SNR of merely 6500 yr. We argue that because this age is inconsistent with the characteristic age ($P/2\dot{P} \sim 20{,}000$ yr) of PSR 1853+01, the radio pulsar believed to be associated with W44, this model does not provide the explanation for the center-filled morphology. We favor the radiative-phase shock model since it can reproduce both the morphology and the age of W44, assuming reasonable values for the initial explosion energy, in the range 0.7–0.9 $\times 10^{51}$ ergs, and an ambient ISM density of between 3 and 4 cm^{-3}.

Subject headings: ISM: abundances — ISM: individual (W44) — nuclear reactions, nucleosynthesis, abundances — shock waves — supernova remnants — X-rays: ISM

1. INTRODUCTION

The study of supernova remnants (SNRs) provides a unique tool for deepening our understanding of the interstellar medium (ISM) and the processes that shape its structure, energetics, and composition. At the time of their death, stars induce a formidable release of energy into the ISM, and a strong shock wave begins to propagate. At early stages of the evolution, the observed emission contains contributions from both the supernova (SN) ejecta and the ISM. One of the major challenges for X-ray spectroscopy of young SNRs is the differentiation and characterization of these two contributions. Knowledge of the composition of SN ejecta is of considerable importance for the constraints it can provide, through the study of nucleosynthesis, on the nature and evolution of the progenitor star. At later stages, SNRs and their evolution are dominated by the interstellar medium. In this article we explore the nature of W44, a middle-aged supernova remnant in the ISM-dominated stage of evolution.

W44 was first discovered as a radio source in a survey by Westerhout (1958), and was observed later by several others (Mills, Slee, & Hill 1958; Edge et al. 1959). It was identified as a possible supernova remnant by Scheuer (1963) because of its shell-like radio structure and its nonthermal radio spectrum. OH and H I absorption measurements (Goss 1968; Goss, Caswell, & Robinson 1971; Radhakrishnan et al. 1972; Knapp & Kerr 1974) have resulted in a more complete mapping of the heavily obscured surroundings of the SNR and have led to the wide acceptance of a distance to the remnant of 3 kpc. The 20 cm VLA image shows a roughly elliptical limb-brightened radio shell with major and minor semiaxes of 15 and 10 pc for this assumed distance (Jones, Smith, & Angellini 1993). Knots and filaments contributing to the emission are also seen; Jones et al. (1993) have interpreted these as arising from the radiative shocks driven into interstellar clouds. The radio emission is nonthermal, with a spectral index of -0.3, and highly polarized ($> 20\%$; Kundu & Velusamy 1972).

There are two radio pulsars in the vicinity of W44. One of them, PSR 1854+00 (Mohanty 1983), is old (10^8 yr), which makes an association between it and the remnant unlikely. The discovery of the other pulsar, PSR 1853+01, is more recent (Wolszczan, Cordes, & Dewey 1991). Taylor, Manchester, & Lyne (1993) give a distance to this pulsar of

[1] Harvard-Smithsonian Center for Astrophysics, 60 Garden Street, Cambridge, MA 02138.
[2] Department of Physics, Columbia University, 550 W 120th Street, New York, NY 10027.
[3] Department of Physics and Astronomy, Rutgers University, P.O. Box 849, Piscataway, NJ 08855-0849.
[4] Tata Institute of Fundamental Research, Homi Bhabha Road, Mumbai, 400 005 India.
[5] Department of Physics, Kyoto University, Kitashirakawa, Oiwake-cho, Sakyo-ku, Kyoto 606, Japan.
[6] Max-Planck-Institut für extraterrestrische Physik, W-8046 Garching bei München, Germany.

3.3 ± 0.3 kpc, while the dispersion-measure distance (Taylor & Cordes 1993) is 2.8 ± 0.1 kpc; both of these are in excellent agreement with the distance estimate to W44 mentioned above. There is a faint radio synchrotron nebula associated with PSR 1853+01 (Jones et al. 1993; Frail et al. 1996), and an X-ray counterpart to the nebula has also been recently announced (Harrus, Hughes, & Helfand 1996), although it accounts for only 3.3% of the total X-ray luminosity of the remnant in the 0.4–2.0 keV band. This is a young pulsar; it exhibits large-amplitude timing noise, and the ratio of the period to the period derivative, the characteristic spin-down age of the pulsar, is $\sim$20,000 yr. Assuming that one can reliably associate the pulsar and the SNR W44, this provides an independent estimate of the remnant's age, which, as we show below, offers an extremely valuable piece of information for discriminating between evolutionary scenarios.

W44 was discovered as an X-ray source by the *Astronomical Netherlands Satellite* (Gronenschild et al. 1978), and has been a popular target of all subsequent X-ray astronomy satellites. Smith et al. (1985) presented the first detailed X-ray imaging observations based on data from the imaging proportional counter (IPC) on board the *Einstein Observatory*. In the soft X-ray band, W44 presents a centrally peaked morphology, more reminiscent of a pulsar-driven synchrotron nebula (like the Crab Nebula) than a shell-type SNR (like the Cygnus Loop). However, the X-ray spectrum of W44 (Jones et al. 1993; Rho et al. 1994) is predominantly thermal in origin, based on the presence of strong emission lines from highly ionized atoms of magnesium, silicon, sulfur, and iron clearly observed by the *Einstein* solid state spectrometer (SSS). Notwithstanding the presence of PSR 1853+01 and its associated synchrotron nebula, W44 belongs to the class of "center-filled" remnants, which show limb-brightened radio shells, centrally peaked X-ray morphologies, and predominantly thermal X-ray spectra.

In the Sedov (1959) model of supernova remnant evolution, the SN blast wave propagates through an isotropic homogeneous ISM. At the shock front, the swept-up material is heated to temperatures of the order of 10^7 K, resulting in a shell-like X-ray morphology with a thermal spectrum. The limb-brightened radio emission comes from compression of the interstellar magnetic field and the accompanying acceleration of electrons, which also occurs at the SNR shock front. This simple model, although apparently successful for many of the known shell-like SNRs, fails to account for remnants such as W44 that have a distinct, centrally peaked X-ray morphology.

Other models have been proposed to explain the observed morphology of W44 and other remnants of this type. In one particular scenario, the remnant is in a later phase of evolution when the blast wave has gone radiative (shock velocities of roughly 300 km s^{-1}; Cox 1972). The radio shell traces the position of the shock front, but since the X-ray emission from the shock front is soft ($kT \sim 10^6$ K) and the line-of-sight ISM column density is significant ($\sim 10^{22}$ atoms cm^{-2}), the outer shell is essentially invisible in the X-ray band (Smith et al. 1985). The X-ray emission comes rather from the hot interior of the remnant, providing a center-filled morphology. This model predicts that W44 should be old and that the X-ray temperature should decrease from the center of the SNR toward the edge. Some support for this scenario comes from the recent discovery of Hα- and S II–emitting optical filaments around the periphery of the X-ray emission (Rho et al. 1994) and an expanding shell of H I emission (Koo & Heiles 1995), indicating the presence of cool gas. In the scenario of White & Long (1991, hereafter WL), the SNR is expanding into a cloudy ISM (as in the ISM models of McKee & Ostriker 1977), and evaporating clouds produce an increased density of hot gas in the interior, giving the centrally peaked appearance. Here the temperature is expected to be relatively uniform throughout the interior.

In this article we explore the implications of these two evolutionary scenarios for W44 using constraints obtained from X-ray imaging and spectroscopic observations from the *Einstein Observatory*, *ROSAT*, and *Ginga*. The next section presents a brief summary of our current knowledge of the SNR in the X-ray band and of the observations used in our analysis. Our models and the analysis techniques that provide the relevant observational constraints are presented in § 3. We apply these constraints to W44 in the context of the two proposed evolutionary scenarios in § 4. A summary of the paper's main points is to be found in § 5.

2. X-RAY OBSERVATIONS OF W44

2.1. *ROSAT PSPC*

The first set of data to be described comes from the position-sensitive proportional counter (PSPC) (Pfeffermann et al. 1986) on board *ROSAT* (Trümper 1983). The PSPC spectral resolution ($\Delta E/E$) was about 45% (FWHM) at 1 keV, and the instrument was sensitive over the energy band 0.1–2.4 keV. W44 was observed by the PSPC in 1991 April. Note that these data were also analyzed by Rho et al. (1994).

We extracted the PSPC data from the *ROSAT* archive and carried out the following reduction procedures. First we applied a time filter to reject data obtained during orbital periods contaminated by solar X-rays scattered into the telescope's field of view by the upper atmosphere. These periods manifest themselves as sudden increases in the total count rate at the beginning or end of the good time intervals supplied as part of the *ROSAT* standard processing. After rejecting these time periods, the deadtime-corrected exposure time was 6726 s. In order to minimize contamination due to particle-induced background, it has been recommended that data be rejected during time intervals when the master veto rate is greater than 170 s^{-1} (Snowden et al. 1994). Since only 3% of our remaining data had an associated master veto rate above this threshold, we decided not to apply an additional time filter to reject those events. We also restricted our analysis to the central 40′ region of the detector.

The W44 source spectrum was extracted from within the region defined by the surface brightness contour corresponding to 10% of the peak brightness. The background region lay outside this, but still came from within the central region of the PSPC (within the window support ring). The background spectrum was corrected for the energy-dependent difference in detector response (mainly due to off-axis vignetting) between the source and background regions and was normalized by the ratio of the solid angle between the regions. After background subtraction, the total PSPC count rate of W44 is 4.22 ± 0.02 s^{-1}. The PSPC spectrum of the entire remnant is shown in Figure 1. A fit to these data using a solar-abundance, collisional equilibrium ionization thermal plasma model (Raymond & Smith 1977

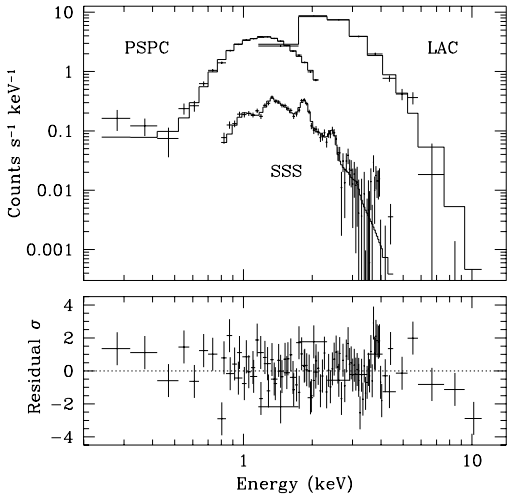

FIG. 1.—Top panel shows X-ray spectra of W44 from the *ROSAT* PSPC, *Einstein* SSS, and *Ginga* LAC with the best-fit single-temperature, single-timescale nonequilibrium ionization model. The residual spectrum (observed data minus best-fit model) is shown in the bottom panel.

[1992 July 27 version], hereafter RS) provided an unacceptable fit, with a χ^2 of 39 for 19 degrees of freedom. In this case, the best-fit temperature, kT, was ~ 1 keV, and the column density, $N_{\rm H}$, was 7.9×10^{21} cm^{-2}.

2.2. *Einstein SSS*

The *Einstein* solid state spectrometer (SSS) has been described in detail by Joyce et al. (1978) and Giacconi et al. (1979); here we provide only a brief discussion of its main characteristics. The SSS was sensitive to X-rays between 0.4 and 4.0 keV, with a nominal spectral resolution (FWHM) varying from 30% at low energies to 4% at high energies. During orbital operations, an unexpected problem of ice formation on the detector window occurred, which caused a time dependence in the low-energy efficiency of the SSS. An empirical model for this effect has been developed based on the analysis of a number of observations of the Crab Nebula taken throughout the course of the *Einstein* mission (Christian et al. 1992); in this work we employ the nominal ice absorption model appropriate to the dates of observation of W44.

The total SSS exposure time on W44 was 22,608 s. The data were acquired in four separate pointings toward two different regions of the remnant. (Note that the field of view of the SSS was about 6′ in diameter, and thus a single pointing did not cover the entire SNR.) The four data sets were compared and, since they were consistent with each other within the statistical errors, summed to form a single spectrum. The separate response functions were averaged (weighting by the exposure time of each pointing). A total of 8072 source photons were detected. In order to account for systematic uncertainties in the ice absorption model, as well as other uncertainties in the SSS calibration, we have added a systematic error equal to 2% of the source intensity in each spectral bin. The minimum energy we consider for this data set is 0.8 keV. The SSS spectrum in Figure 1 shows obvious emission lines from Kα transitions of highly ionized atoms of magnesium, silicon, and sulfur, which clearly points to a thermal origin for the X-ray emission. Nevertheless, this spectrum cannot be fitted well by a simple solar-abundance RS thermal plasma emission model. The reduced χ^2 of 4.5 obtained in this case for $kT \sim 0.9$ keV and $N_{\rm H} = 7.4 \times 10^{21}$ cm^{-2} indicates that a more detailed analysis, taking into account effects such as nonequilibrium ionization, is necessary.

2.3. *Ginga LAC*

The major experiment on *Ginga* (Makino et al. 1987) was the Large Area Counter (LAC) (Turner et al. 1989), an array of eight sealed proportional counters with a total geometric collecting area of 4000 cm^2, mechanically collimated to a field of view of roughly 1° by 2° (FWHM). The efficiency of the LAC for collecting X-rays was greater than 10% over the 1.5–30 keV band. The lower energy limit was defined by the thickness of the Be window material (~ 62 μm), while the high-energy limit arose from the finite active depth of the proportional-counter gas volume. These detectors had an energy resolution of 18% (FWHM) at about 6 keV. With its very low internal background rate and large effective area, the LAC was a very sensitive instrument for carrying out X-ray spectral studies.

No direct pointing of W44 was made by *Ginga*. Rather, we have extracted data on the source from a scan of the Galactic plane carried out on 1988 September 12. Scan data were taken in MPC2 mode, which combined data from the top and middle layers of the LAC and summed data from four detectors into one before telemetering to the ground. The two spectra so obtained were summed during data reduction. Background was determined from source-free regions of the scan on either side of W44. The effective exposure time was low (1984 s); however, the source is bright (~ 15 counts s^{-1}), and the X-ray spectrum is well defined from 1.5 keV to 10 keV. The spectrum is soft, consistent with a RS thermal model with $kT \sim 0.75$ keV and an interstellar column density of $\sim 10^{22}$ cm^{-2}. There is no evidence for any harder emission component in the *Ginga* data. We set an upper limit (3 σ) of 3.6×10^{-12} ergs cm^{-2} s^{-1} to the 2–10 keV flux of a Crab-like power-law component ($dN/dE \sim E^{-2.1}$) contributing to the *Ginga* spectrum of W44.

2.4. *Other Observations*

During the initial phases of this study, we explored the possibility of using X-ray observations of W44 from other archival data sources, namely, from the *Einstein Observatory* and *EXOSAT*. After careful evaluation it became clear that these data would not be useful in our study. We review our arguments for arriving at this conclusion below.

The *Einstein* imaging proportional counter (IPC) is similar to the *ROSAT* PSPC in many respects. The major advantage of the IPC over the PSPC is its higher energy cutoff (4.5 keV vs. 2.4 keV). This advantage, however, is largely offset by the IPC's poorer energy resolution and image quality, and the large uncertainty in its calibration, which limits its usefulness for detailed spectral analysis. In our preliminary spectral fits, it was found that the IPC global spectrum was consistent with that from the PSPC and SSS, although the best-fit χ^2 for the IPC data was formally unacceptable. Although consistent with the other data, the IPC spectrum does not provide additional constraints on the model, and thus we reject it as being redundant.

Data from the medium energy (ME) proportional counters on *EXOSAT* are available through the High Energy Astrophysics Science Archive maintained by the

Goddard Space Flight Center (GSFC). The data in this archive have undergone a standard reduction procedure to produce background-subtracted spectral files for analysis. The processing flag for the ME spectrum of W44 is listed as quality 2, which indicates a major problem with the reliability of the data. Indeed, the ME spectrum of W44 shows a hard component above about 5 keV and a reasonably strong Kα iron line, both of which are entirely absent in the *Ginga* LAC spectrum.

The problem with the standard background subtraction for this W44 data was identified by Jones et al. (1993), who examined the raw ME data and found that a significant fraction of it was contaminated by irregular count rate flares, presumably induced by penetrating charged particles. After rejecting the data from the most seriously affected detectors, Jones et al. (1993) obtained good fits to the ME data of a single-temperature RS thermal model with $kT \sim 0.9$ keV and $N_{\rm H} \sim 10^{22}$ cm^{-2}. These results are consistent with those derived using the *Ginga* data. Because we had no access to the raw *EXOSAT* data and since the *Ginga* LAC covers the same energy band and is therefore fully complementary, we decided to exclude the ME data altogether.

In their complex analysis of W44, Rho et al. (1994) use the contaminated ME data obtained directly from the GSFC archive. This explains why these authors require a high-temperature component in their model fits. In our view, it also likely invalidates the conclusions they arrive at concerning their best-fitting NEI spectral model (i.e., shock temperature, ionization timescale, and assumptions about electron-ion temperature equilibration timescales).

3. NONEQUILIBRIUM IONIZATION MODELING AND ANALYSIS

Accurate plasma diagnostics are the key to our understanding of the physical phenomena occurring during supernova remnant evolution. At the simplest level, measurements of plasma temperature and elemental abundances allow one to derive quantitative values for the plasma density in the SNR from the intensity and brightness distribution shown by broadband X-ray images. Furthermore, as we show below, the remnant's radius, temperature, and density are essential quantities for understanding its dynamical state. The relative abundance ratios of the X-ray–emitting plasma, as determined by spectroscopy, can indicate the presence of reverse-shocked ejecta, again providing clues to the evolutionary state of the remnant. The driving force behind the detailed spectral fits we pursue in the following section is a derivation from the observational data of the most accurate values possible for the thermodynamic quantities, of which the most important is the mean electron temperature.

Interpretation of SNR X-ray spectra is complicated by the nonequilibrium processes that occur in low-density shock-heated plasmas and that necessitate detailed time-dependent models of the spectral emissivity. One important influence on the thermodynamic state of the plasma is the fact that the ions are not instantaneously ionized to their equilibrium configuration at the temperature of the shock front. Rather, the timescale for attaining full equilibrium ionization is comparable to the remnant dynamical timescale. Numerous authors have incorporated this nonequilibrium ionization (NEI) effect into models of SNR spectral emissivity. Here we use the matrix inversion method developed by Hughes & Helfand (1985) to solve for the time-dependent ionization fractions, and couple it to the RS plasma-emission code (see Hughes & Singh 1994 for more details). The column density of neutral hydrogen along the line of sight, $N_{\rm H}$, is included as a fitting parameter, using cross sections and ISM abundances from Morrison & McCammon (1983).

3.1. *Single-Temperature, Single-Timescale NEI model*

The simplest NEI model assumes that the X-ray–emitting plasma was impulsively heated to temperature kT some time t ago. The temperature, defined as the kinetic state of the electrons, is assumed to remain constant. The ionization state depends on the product of the electron density and age: i.e., the ionization timescale, $\tau_i \equiv n_e t$. We refer to this as the single-temperature, single-timescale NEI model, and we apply it here to the spectra from the entire remnant.

The observed spectra constrain the electron temperature in the SNR mainly through the shape of the continuum emission, which is independent of the ionization state, equilibrium or otherwise, to at least first order. (In fact, a model-independent analysis of these data using a parameterized bremsstrahlung function plus several Gaussians to describe the line emission yields a similar value, ~ 1 keV, for the electron temperature.) The ionization timescale is determined by the centroid energies of the various Kα lines (which are, after all, blends of lines from hydrogen-like ions, helium-like ions, etc., and so depend sensitively on the ionization state) that appear in the spectral band, Ne, Mg, Si, and S, in particular. The relative intensities of these emission lines derived from the model fits can, in principle, constrain individual elemental abundances. In practice, some of the individual contributions are not easily separated, especially for those species that are primarily continuum contributors. Therefore, we have fixed abundances for the elements He, C, N, and O to the solar values relative to hydrogen. The abundances of the other elemental species were allowed to vary freely. We adopt as solar abundances the values given by RS.

Figure 1 shows the data and best-fit NEI model obtained when the three data sets are fitted jointly. The minimum χ^2 is 137.4 for 92 degrees of freedom. The χ^2 associated with the PSPC data is 25.4 (22 data bins), for the SSS data it is 87.0 (72 data bins), and for the LAC data it is 25 (11 data bins). The overall normalization of the spectral data provides a value for the emission measure of the hot plasma in W44 as $n_{\rm H}^2 V/(4\pi D^2) = (1.76 \pm 0.37) \times 10^{13}$ cm^{-5}. We use a value of 1.09 for the ratio $n_e/n_{\rm H}$. The best-fit values for the global spectral parameters are temperature, $kT = 0.88 \pm 0.14$ keV, ionization timescale, $\tau_i = 2.0^{+4.3}_{-0.7} \times 10^{11}$ cm^{-3} s, and column density, $N_{\rm H} = 1.0^{+0.6}_{-0.2} \times 10^{22}$ atoms cm^{-2}. The quoted error bars are at the 90% confidence level for three interesting parameters ($\Delta\chi^2 = 6.25$). Figure 2 shows graphically how χ^2 varies with each of these global parameters (also allowing all other parameters to vary freely). Table 1 provides a numerical summary of the abundance results. The second column gives the best-fit elemental abundances relative to their cosmic values. The third column shows the errors in abundances determined with the temperature, ionization timescale, and column density fixed at their best-fit values. The remaining columns give the errors in abundances arising from the variation in the global spectral parameters as shown in Figure 2.

The ionization timescale we derive for W44 is similar to

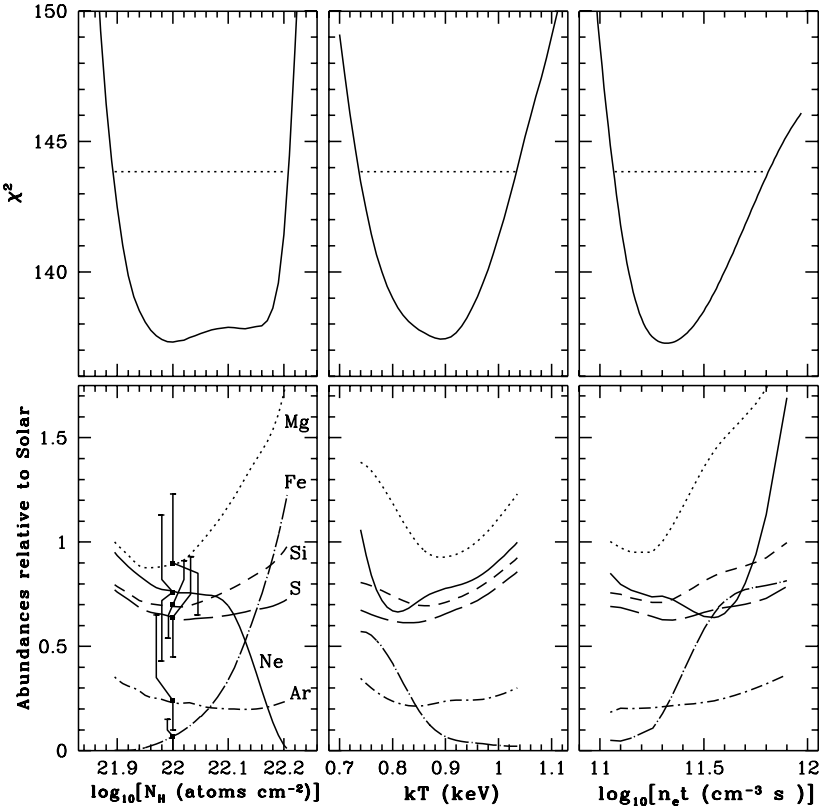

FIG. 2.—Effect of variation in column density (N_H), temperature (kT), and ionization timescale ($n_e t$) on the best-fit elemental abundances of the various species considered from fits to the W44 X-ray spectra using the nonequilibrium ionization model. The top three panels show the change in χ^2 with the independent variation of each spectral parameter. The 90% confidence interval (for three interesting parameters) is shown in each panel as a dashed line ($\chi^2_{min} + 6.25$). The variations of elemental abundance (relative to the appropriate solar value) are shown in the bottom panels. Error bars are plotted at the best-fit values and represent the random error at 90% confidence.

that expected from a middle-aged remnant (such as N132D in the LMC; see Hwang et al. 1993) and is indicative of a plasma that is underionized for its temperature. From the *ROSAT* image, we estimate the mean electron density in the hot plasma (see below) to be $\langle n_e^2 \rangle^{1/2} \simeq 0.4$ cm^{-3}. Combined with the ionization timescale, this suggests an "age" of the order of 15,000 yr, in good agreement with other estimates of the age of W44 and its associated pulsar PSR 1853+01 (see below).

3.2. *Radial Temperature Gradient*

Some evolutionary scenarios for SNRs (e.g., Sedov 1959) predict significant radial variations in the plasma temperature, while others (e.g., WL) do not. We have used the *ROSAT* PSPC data to constrain the allowed range of temperature variation in W44 in the following approximate manner. Two PSPC spectra were extracted: one from within a radius of 6′.7 and the other from outside this region. Note that the boundary between the regions was chosen so that each spectrum had roughly the same total number of detected counts; the results are not sensitive to the exact position of the boundary. Each PSPC spectrum was fitted to an independent NEI model, and the sum of these NEI models was required to fit the LAC and SSS data. These latter two data sets were assumed to be representative of the entire remnant (which is strictly correct for the LAC data, but only approximately true for the SSS). The NEI models were constrained to have the same abundances, column density, and ionization timescale, with values fixed to the best-fit ones determined above, while the temperatures and intensity normalizations of the models describing the two regions were allowed to vary independently. We obtain a

TABLE 1

ELEMENTAL ABUNDANCES OF W44

SPECIES	BEST FIT RELATIVE TO ⊙	RANDOM ERROR	ERROR DUE TO VARIATION WITH:		
			N_H	$n_e t$	kT
Ne	0.76	$^{+0.35}_{-0.35}$	$^{+0.18}_{-0.78}$	$^{+0.20}_{-0.15}$	$^{+0.40}_{-0.10}$
Mg.....	0.90	$^{+0.33}_{-0.25}$	$^{+0.80}_{-0.10}$	$^{+0.50}_{-0.10}$	$^{+0.60}_{-0.10}$
Si	0.70	$^{+0.21}_{-0.16}$	$^{+0.25}_{-0.05}$	$^{+0.15}_{-0.05}$	$^{+0.20}_{-0.10}$
S	0.64	$^{+0.28}_{-0.20}$	$^{+0.15}_{-0.05}$	$^{+0.15}_{-0.05}$	$^{+0.15}_{-0.05}$
Ar.....	0.24	$^{+0.40}_{-0.15}$	$^{+0.15}_{-0.05}$	$^{+0.10}_{-0.05}$	$^{+0.15}_{-0.05}$
Fe.....	0.07	$^{+0.08}_{-0.07}$	$^{+1.10}_{-0.07}$	$^{+0.35}_{-0.07}$	$^{+0.65}_{-0.07}$

better fit if the inner region is somewhat hotter than the outer region. At 90% confidence, the temperature of the inner region is constrained to be between 10% and 20% higher than the temperature of the outer region. This analysis indicates that there is little variation of temperature with position in the remnant, a result that is consistent with previous studies (Rho et al. 1994).

3.3. *Multiple NEI Components*

In addition to the simple single-temperature, single-timescale NEI model discussed above, we also have investigated the possibility that the X-ray–emitting plasma in W44 is in a more complex state. First, we looked for evidence that the ionization state varies as a function of elemental species. In this study we had two ionization timescales as free parameters, one for a particular individual species (Ne, Mg, Si, S, Ar, and Fe, each in turn) and the other for all the remaining elemental species. Fits were carried out with the other relevant spectral parameters (kT, $N_{\rm H}$, and abundances) constrained to be the same for all species and allowed to vary freely. The derived χ^2 values were compared to the single-temperature, single-timescale results to assess the significance of the introduction of the new parameter. None of the elemental species for which we pursued this analysis showed a statistically significant difference, suggesting that the various elements contributing to the X-ray emission are uniformly mixed throughout the plasma.

We also carried out fits of a two-component NEI model to the entire spectrum to see whether our data required that the plasma in W44 be multiphase. The components had the same starting abundance as found in the one-component NEI analysis and identical absorbing column density. We assumed that the media were in pressure equilibrium, which allowed us to relate the ionization timescales and temperatures as $\tau_{i,2} = \tau_{i,1}\, T_1/T_2$. Note that we also made the implicit assumption that the two components were shocked at the same time. With this condition, only two additional free parameters were introduced: the second temperature and the ratio of emission measures between the two media. We explored values for the temperature of the second component from 0.5 to 5 keV and the ratio of emission measure from 0.1 to 10. Over this range of parameter space, no statistically significant reduction in χ^2 was observed, although equally good fits were obtained in many cases. Our data allow a second component with $kT = 2$ keV only if its emission measure is less than $\sim$3% that of the main component. The allowed emission measure for the addition of a 5 keV component is even more restricted, less than 0.5% of the main component. Because of the significant interstellar cutoff, our limits on gas at temperatures with $kT < 0.5$ keV are rather weak.

3.4. *Volume, Density, Pressure, and Mass Estimates*

In the soft X-ray band, W44 is roughly elliptical in appearance, with a long dimension of 33′ and a short one of 20′. We estimate the volume of the remnant as an ellipsoid with principal axes in the plane of the sky of sizes as observed. The length of the third axis is some factor, α, times the size of the observed short dimension. This corresponds to a volume of $V = 1.3 \times 10^{59} \alpha D_{3\ {\rm kpc}}^3\ {\rm cm}^{-3}$ for the nominal distance to W44 of 3 kpc.

The root mean square electron density can be determined simply from the fitted emission measure (see § 3.1) and the volume. We obtain

$$\langle n_e^2 \rangle^{1/2} = 0.42(\alpha f D_{3\ {\rm kpc}})^{-1/2}\ {\rm cm}^{-3}\ , \qquad (1)$$

where f is the volume filling factor of the hot plasma. The uncertainty in $\langle n_e^2 \rangle^{1/2}$ from errors in the fitted emission measure alone is ± 0.06 cm^{-3}. The average thermal pressure in the remnant is roughly 1.1×10^{-9} ergs cm^{-3}, assuming that the ion and electron temperatures are equal.

The mass of X-ray–emitting hot plasma is given by

$$M = 56(\alpha f)^{1/2} D_{3\ {\rm kpc}}^{5/2}\ M_\odot\ . \qquad (2)$$

3.5. *Abundances*

Vancura et al. (1994) argue for the use of depleted abundances in interpreting the X-ray spectra of SNRs, owing to the long timescales for grain destruction within the shock-heated gas. In their models, the proportion of intact silicate and graphite grains that remain after being engulfed by a blast wave depends strongly on the shocked column density, N_S, but only weakly on the shock velocity. For W44, we approximate N_S by the product of the rms density and the mean observed radius, which gives a value of $N_S \sim 1.5 \times 10^{19}$ cm^{-2}. The fraction of initially depleted mass remaining in the solid phase for this shocked column is 30%–45% (Vancura et al. 1994), implying that the observed abundances of Mg, Si, S, and Fe in W44 should be slightly below solar (abundances of 60%–80%). The relatively inert elements Ne and Ar should show no depletion.

Our best fit to the X-ray spectrum of W44 implies elemental abundances that are close to or somewhat below solar values (except for iron), and in general agreement with the picture sketched above. The strongest apparent depletion is observed for iron, although we are wary of this result because of uncertainties in the atomic physics of iron L-shell emission. It is also true that the iron abundance observed varies dramatically with changes in the global spectral-fit parameters, as clearly shown in Figure 2. For $N_{\rm H}$ values slightly higher than the best-fit one (but still within the allowed range), all derived elemental abundances are within a factor of $\sim$2 of solar.

On the other hand, it is slightly puzzling that the observed abundance pattern shows no clear evidence for the presence of SN ejecta. Models of nucleosynthesis in massive stars (ZAMS masses of 13–25 $M_\odot$) predict, for example, the ejection of 0.047–0.116 $M_\odot$ of Si and 0.026–0.040 $M_\odot$ of S (Thielemann, Nomoto, & Hashimoto 1996). For W44 we observe in total only about 0.03 $M_\odot$ of Si and 0.01 $M_\odot$ of S, and most of this, we have just argued, can be attributed to the swept-up interstellar medium. Perhaps this suggests that the progenitor of W44 is less massive than 13 $M_\odot$, although a lower bound of 8 $M_\odot$ seems necessary in order to produce the neutron star of the associated PSR 1853+01 (Wheeler 1981). The fate of the metals ejected by a SN is also complex, due to adiabatic cooling during the initial free-expansion phase, subsequent heating by the reverse shock, radiative cooling, the disruption of the ejecta, and so on. As interesting as these issues are, addressing them is beyond the scope of this work, and will require observational data of considerably higher spatial and spectral quality than are currently available.

4. EVOLUTIONARY STATE OF W44

The radio image of W44 (Jones et al. 1993; Frail et al. 1996) shows an elliptically shaped, limb-brightened mor-

phology, with a size of 34′.8 × 24′.4. In the models considered below, we use the boundaries of the radio emission to delineate the position of the blast wave, employing the mean radius $R_s = 13.1$ pc $(\theta_s/15')(D/3$ kpc) in our calculations. The X-ray emission from W44 is also elliptical in shape, although centrally peaked, and lies entirely within the radio shell. The elliptical nature of the emission region implies that the models used, which are spherically symmetric, cannot be completely valid. Nevertheless, as a good first approximation we compare the radially averaged surface brightness profile from the *ROSAT* PSPC with predictions from the models.

4.1. *The W44/PSR 1853+01 Association*

In the PSR 1853+01 discovery paper (Wolszczan et al. 1991), the arguments for associating this pulsar and the SNR W44 were first laid out: these were positional coincidence, agreement in inferred distance, the youth of the pulsar as indicated by the observed large-amplitude timing noise, and agreement between the characteristic spin-down age of the pulsar and the dynamical age of the remnant. More recent research has provided additional strong evidence to support this association. Frail et al. (1996) have imaged the radio synchrotron nebula around PSR 1853+0.1, which they find to show an unusual cometary morphology, with the pulsar located near the narrow (southern) end of the nebula. The thermal pressure necessary to confine the radio nebula is roughly 6×10^{-10} ergs cm^{-3}, which, while several orders of magnitude larger than the pressure of the interstellar medium in general, is within a factor of 2 of our pressure estimate for the hot gas in W44 (see § 3.4). This measurement can leave little doubt that PSR 1853+0.1 lies within the hot X-ray–emitting plasma of W44 and that, consequently, the pulsar and the SNR were formed in the same supernova explosion.

As we show below, just *when* that SN explosion occurred is critical to our understanding of the evolutionary state of W44. One estimate is provided by the spin-down age of the pulsar. The spin-down of pulsars is believed to follow the relation $\dot{\nu} = -K\nu^n$, where ν is the rotation rate, n is the braking index, and K depends on the properties (such as the moment of inertia and magnetic field) of the neutron star. A value of $n = 3$ is expected if the pulsar's rotational energy is lost purely through radiation from a dipole magnetic field. Assuming K and n to be constant, one derives the age t of the pulsar by

$$t = \frac{P/\dot{P}}{(n-1)}\left[1 - \left(\frac{P_0}{P}\right)^{n-1}\right], \qquad (3)$$

in terms of the initial spin period P_0, the current period P, and period derivative $\dot{P}$. The braking index has been measured for three young pulsars, the Crab (PSR B0531+21), PSR B0540−69, and PSR B1509−58, and all show values of less than 3 for n, being 2.51 ± 0.01 (Lyne, Pritchard, & Smith 1993), 2.20 ± 0.02 (Boyd et al. 1995), and 2.837 ± 0.001 (Kaspi et al. 1994), respectively. Recently, Lyne et al. (1996) measured the braking index of the Vela pulsar, which is roughly 10 times older than the pulsars mentioned above and in that sense most closely resembles PSR 1853+0.1, and they find a surprisingly low index value of $n = 1.4 \pm 0.2$. Nonetheless, Lyne et al. (1996) claim that the age derived using this braking index and a low initial-spin period (20 ms, the estimated initial spin period of the Crab) results in a value that is consistent with other estimates of the age of the Vela SNR.

The radio timing parameters of PSR 1853+0.1 are $P = 0.26743520599(6)$ s and $\dot{P} = (208.482 \pm 0.006) \times 10^{-15}$ s s^{-1} (A. Wolszczan 1995, private communication). Assuming a low initial spin period of 20 ms, we estimate an age for PSR 1853+0.1 of 2.65×10^4 yr, with $n = 2.5$. If $n = 1.5$, the age estimate is increased significantly, to 5.9×10^4 yr. For PSR 1853+0.1 to be younger than ∼10,000 yr, it must have been born as a slow rotator, with a spin period $\gtrsim 200$ ms, or have undergone an unusual spin-down history. Although not inconceivable, this would make the pulsar in W44 different from the other known pulsars in SNRs discussed above.

4.2. *The White & Long Model*

The White & Long (1991) similarity solution for the evolution of SNRs invokes a multiphase interstellar medium consisting of cool dense clouds embedded in a tenuous intercloud medium. The blast wave from a SN explosion propagates rapidly through the intercloud medium, engulfing the clouds in the process. In this model, the clouds are destroyed by gradually evaporating on a timescale set by the saturated conduction heating rate from the postshock hot gas. Since this timescale can be long, it is possible for cold clouds to survive until they are well behind the blast wave, which as they evaporate can significantly enhance the X-ray emission from near the center of the remnant.

The timescale for cloud evaporation is one of two parameters in the White & Long (WL) model which are in addition to the three other parameters (explosion energy E_0, ISM density n, and SNR age t) characterizing the standard Sedov solution. This timescale, expressed as a ratio of the evaporation timescale to the SNR age, $\tau_e \equiv t_{\rm evap}/t$, can depend on various factors, such as the composition of the clumps and the temperature behind the shock front. The other new parameter, C, represents the ratio of the mass in clouds to the mass in intercloud material. For appropriate choices of these two new parameters, the model can produce a centrally peaked X-ray emission morphology. Alternatively, other choices of τ_e and C can reproduce the standard Sedov solution. This model has been applied to the centrally peaked remnants W28 and 3C400.2 (Long et al. 1991), as well as to CTA 1 (Seward, Schmidt, & Slane 1995).

We searched the C-τ_e plane of parameter space to determine which values gave a good match to the W44 radial X-ray surface brightness profile. We integrated the differential equations from the WL similarity solution to obtain the radial run of temperature and density throughout the interior of the remnant. These functions were normalized to their values at the shock front. The temperature at the shock front, T_s, was related to the emission-measure–weighted temperature $\langle T \rangle$ (which is the quantity we measured) using equation (23) of WL. The density at the shock front, n_s, was scaled to match the observed emission measure of X-ray–emitting gas in W44. For each set of C and τ_e values, appropriate values for T_s and n_s were calculated. With these values and the radial run of temperature and density, it was possible to calculate the radial X-ray surface brightness profile. For each radial bin in the SNR model, a RS plasma model of appropriate temperature was calculated, and the resulting photon spectrum was multiplied by the energy-dependent ISM absorption function,

assuming our best-fit column density. The absorbed spectrum was convolved with the PSPC efficiency and spectral resolution functions, then projected to the plane of the sky. This was iterated over all radial bins of the model.

Values of C and τ_e in the ratio of approximately 2.5:1 for $5 \lesssim C \lesssim 100$ provided reasonable profiles. In Figure 3 we show the observed PSPC surface brightness profile along with several representative WL models. Dashed curves bracket the range of acceptable solutions, with the top one being too centrally peaked, while the bottom one is too limb-brightened. The three curves near the center show examples of good fits.

The dependence of remnant age t on shock radius and temperature T_s in the WL model is identical to that of the Sedov solution:

$$t = 5490 \text{ yr} \left(\frac{\theta_s}{15'}\right)\left(\frac{D}{3 \text{ kpc}}\right)\left(\frac{kT_s}{1 \text{ keV}}\right)^{-1/2}, \quad (4)$$

which solution explicitly includes a functional dependence on distance D. For the allowed range of C and τ_e values, the shock temperature varies between 0.53 and 0.95 keV, including the observational error in kT. This yields an age for W44 of between 5600 and 7500 yr, which is similar to previous estimates of the age of W44 based on applications of the WL model (Rho et al. 1994). The square-root dependence of t on kT_s means that the temperature would have to be an order of magnitude less than the value we actually measured to increase the remnant's age by a factor of 3. We can think of no systematic effect in our data or analysis that could result in such an enormous change in the mean temperature of W44. Note that the age of the remnant in this scenario also depends on distance. However, in order for W44 to be $\sim$20,000 yr old, the remnant would need to be 2.5 times farther away than the accepted distance of 3 kpc. This too is highly unlikely.

Although this model appears to reproduce the intensity and morphology of W44, it predicts an age that is much less than the characteristic age of the associated pulsar. In addition, we find that the estimated initial explosion energies of the acceptable WL models is rather small, 0.11–0.16 $\times$ 10^{51} ergs. These two results considerably weaken the plausibility of the WL model as an accurate description of the SNR W44, particularly in comparison to the model we discuss next.

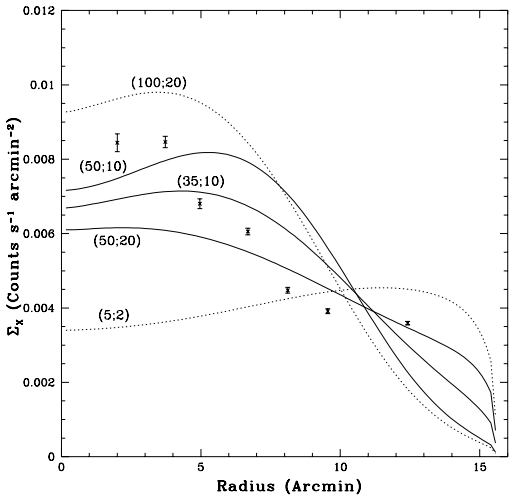

FIG. 3.—Radial X-ray surface brightness profile of W44 from the *ROSAT* PSPC (the seven data points with statistical error bars) compared to the White & Long (1991) similarity solution for the evolution of SNRs in a cloudy interstellar medium. The solid curves show acceptable fits, while the dashed curves indicate the extremes of the allowed solutions. These models all predict a young age (5600–7500 yr) and low explosion energy (0.11–0.16 $\times$ 10^{51} ergs) for W44.

4.3. *Radiative Shock Model*

To study this alternative evolutionary scenario quantitatively, we use a one-dimensional, spherically symmetric, hydrodynamic shock code (Hughes, Helfand, & Kahn 1984). We include radiative cooling parameterized by temperature, as in Raymond, Cox, & Smith (1976), for material with solar abundances. Models were generated with a range of values for the initial explosion energy E_0 and ambient ISM hydrogen number density n, assumed to be homogeneous, isotropic, and free of magnetic fields. For completeness, we have considered two extreme cases for the exchange of energy between shock-heated ions and electrons: (1) rapid equilibration, in which the electrons and ions attain the same temperature instantaneously at the shock front, and (2) equilibration on a timescale set by Coulomb collisions. We find no difference between these for the models that best describe W44, and so we only quote results for the Coulomb equilibration models.

The hydrodynamic calculation was initiated using a homologously expanding, uniform-density shell of ejecta, with a total mass of 10 $M_\odot$ extending over a small spatial extent (from the center of the explosion to a radius of 0.2 pc). At the ages of interest for our modeling of W44, the reverse shock has passed completely through the ejecta, fully thermalizing it. It is well known that a decelerating ejecta shell is subject to Rayleigh-Taylor instability, and observations of young ejecta-dominated SNRs such as Cas A and Tycho show clear evidence that this instability indeed operates in nature. The effect of the instability is to cause significant clumping of the ejecta shell that ultimately results in its fragmentation and disruption. Our simple one-dimensional calculation is unable to model this effect. However, our interest is in studying the onset of dense shell formation at the blast wave, not the fate of the SN ejecta, so this limitation in our calculations is not important. When calculating the projected surface brightness, we remove radial bins containing the modeled ejecta, replacing them with an extrapolation of the temperature and density profile from the solution farther out, guided by the radial run of temperature and density expected from the Sedov (1959) solution. This effectively removes the ejecta from the calculation. In practice, much of the ejecta should remain within the interior of the remnant and, by increasing the metallicity of the gas, enhance the central X-ray emission. Whether the centrally peaked brightness of W44 and other SNRs in this class can be explained at least partially by enhanced metallicity in the remnant interior is beyond the scope of the current study. We will be exploring this issue in future work by searching for abundance gradients using spatially resolved X-ray spectral data.

We initially explored values for E_0 and n, searching for model remnants that attained radii between 12 and 14 pc in ages of between 19,000 and 25,000 yr. This requirement largely constrained the ratio of E_0/n to be $\sim$0.2–0.4 $\times$ 10^{51} ergs cm^3. Next, this range of model parameters was explored more finely in order to find model SNRs that reproduced both the measured X-ray intensity and a centrally peaked surface brightness profile. The model tem-

perature and density profiles were projected as above, using the best-fit ISM column density ($N_H = 1.0 \times 10^{22}$ atoms cm^{-2}) to obtain surface brightness profiles in terms of PSPC counts s^{-1} arcmin^{-2} for comparison to the data. Appropriate values of E_0 in the range 0.1–2 $\times$ 10^{51} ergs and n in the range 0.25–11 cm^{-3} were considered. Best-fit solutions to the W44 data were obtained for $E_0 \approx 0.7$–0.9×10^{51} ergs and $n \approx 3$–4 cm^{-3}. Figure 4 shows the radial X-ray surface brightness profiles of several of these acceptable models.

The curves on Figure 4 labeled *a* and *b* show how the X-ray surface brightness profile varies with age. The top curve shows a model with $E_0 = 0.9 \times 10^{51}$ ergs and $n = 3.0$ cm^{-3} at 19,400 yr, and the bottom curve is the same model at 25,200 yr. In these models there is a dense shell of radiatively cooled ISM at radii of 12.0 pc (*a*) or 12.5 pc (*b*) at the outer edge of the remnant. Inside this shell the temperature rises slowly, increasing from about 10^6 K just inside the shell to 10^7 K near the center. Over the same radial range the density shows a gradient of the opposite sign, decreasing from the edge of the remnant in toward the center. The centrally bright profile is a result of absorption of soft X-rays from near the remnant edge by the large column density to W44. The harder photons from the hotter gas in the interior are preferentially less absorbed, and thus, although the matter density is less there, it has a higher observed emissivity. The other curves in Figure 4 show the X-ray brightness profiles of models with other values for E_0 and n. (Note that we ran our shock model for a fixed explosion energy and age and found that different ISM densities yielded final remnant radii that differed by the observed ellipticity of W44, but still yielded roughly centrally peaked morphologies.)

We estimated nonequilibrium ionization effects on the broadband X-ray surface brightness profile of the radiative phase model in the following manner. For each interior radial shell in the SNR model, we integrated the time history of electron density to form the radial run of the ionization timescale, τ_i. The values of τ_i so determined, plus the final-state value of kT, were used with the single-timescale, single-temperature NEI model to predict the X-ray emissivity through the remnant interior, and then to formulate the projected surface brightness profile in the manner described previously. (This approximation differs from a full-up NEI model only to the extent that the temperatures of individual radial shells may have changed with time. We verified that this was a small effect by comparing the final-state temperature in radial bins of the model with the time-averaged temperature and found that they differed only slightly, the time-averaged temperature being somewhat higher.) The NEI brightness profile for one particular model is shown in Figure 4. It differs from the corresponding equilibrium ionization case by less than 10%, confirming that NEI effects on the modeled brightness profile are minor and that the results presented above are robust. We note that the emission-measure–weighted mean ionization timescale of the NEI model shown in Figure 4 is $\sim 9 \times 10^{11}$ cm^{-3} s, which is in reasonable agreement with the observed value for W44 given the simplicity of the model.

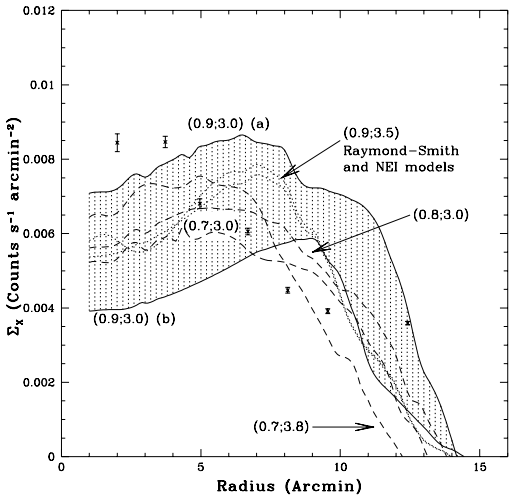

FIG. 4.—Radial X-ray surface brightness profile of W44 from the *ROSAT* PSPC compared to radiative-phase shock models. Curves are labeled with the explosion energy (in units of 10^{51} ergs) and ambient ISM density (cm^{-3}) of the model as E_0, n. The two curves labeled *a* and *b* delineating the dotted region show how the profile varies with remnant age from 19,000 yr (*a*) to 25,000 yr (*b*). All these models are consistent with the spin-down age of the associated pulsar PSR 1853+01, $P/2\dot{P} \sim 20000$ yr.

It has occasionally been suggested that shock models would provide a poor explanation of the centrally peaked SNRs, since such models are expected to show significant radial temperature gradients. The emission-measure–weighted projected temperature of our model, *a* in Figure 4, does show a larger variation in temperature than the 10%–20% from the PSPC data (see § 3.2). The projected temperature in this model varies by about 50% from the center to the edge. One possible solution to this problem could be provided by including thermal conduction processes (e.g., Cui & Cox 1992; Shelton & Cox 1995; Smith 1996), which can have the effect of smoothing out strong temperature gradients. Although promising, studies of this kind are beyond the scope of the current article and are deferred to future research.

The emission-measure–weighted average temperatures of the acceptable shock models, in the range of 0.4–0.5 keV, are also slightly lower than the observed average temperature value of $kT = 0.88 \pm 0.14$ keV from the current data. An independent estimate of the mean temperature for the hot plasma in W44 was obtained by Harrus et al. (1996) from a preliminary analysis of *ASCA* data, which gave a somewhat lower result, $kT = 0.5 \pm 0.2$ keV. Averaging these two independent measurements produces a result for the temperature of W44 that is slightly more consistent with the model predictions, although still somewhat high. Clearly, more careful analysis of the *ASCA* data, plus additional modeling along the lines mentioned in the preceding paragraph, will be crucial in furthering our understanding of the nature of W44 and other filled-center remnants.

All things considered, it is remarkable that this simple model, a function of only three parameters, reproduces both the observed intensity of the remnant and, at least to first approximation, the centrally peaked X-ray brightness profile. The derived parameters, in particular an explosion energy of $\sim 0.9 \times 10^{51}$ ergs, are physically quite plausible. And since the remnant's age is similar to the characteristic age of the pulsar, there is no need to invoke an unusual evolutionary scenario for the spin-down of the pulsar. Because of these considerations, we favor this, the radiative phase shock model, as the interpretation of the center-filled X-ray emission from W44.

This model also accounts quite naturally for the massive, high-velocity shell of H I gas that has been observed sur-

rounding the X-ray–emitting region of W44 (Koo & Heiles 1995). The shell's velocity is estimated to be 150 km s^{-1} and its mass $\sim 350\ M_{\odot}$, with large uncertainties. Although Koo & Heiles (1995) did explore the possibility that the H I shell was a consequence of W44 being in the radiative phase of evolution, they rejected this interpretation through a belief that the centrally peaked X-ray emission from W44 could not be reconciled with the standard radiative model. Our work here has shown that this is just not true; in fact, the radiative phase model is the preferred explanation for the nature of W44. The cool shell in our radiative phase models has a mass within the range of ~ 550–$900\ M_{\odot}$ and expansion velocities of 100–120 km s^{-1} (depending on E_0 and n), values that are in good agreement with the H I observations.

5. SUMMARY

In this article we have presented an analysis of X-ray data from the *Einstein* SSS, the *ROSAT* PSPC, and the *Ginga* LAC on the supernova remnant W44. These spectral data are well described by a single-temperature, single-timescale nonequilibrium ionization model with temperature 0.88 ± 0.14 keV and ionization timescale $2.0^{+4.3}_{-0.7} \times 10^{11}$ cm^{-3} s, observed through a large absorbing column density, $N_{\rm H} = 1.0^{+0.6}_{-0.2} \times 10^{22}$ atoms cm^{-2}. All elemental abundances are close to the solar values, with iron showing possibly significant depletion.

Morphologically, W44 belongs to the class of SNRs that have clear shell-like structures in the radio but are centrally peaked in the X-ray band and exhibit thermal X-ray spectra. We have examined in detail two proposed scenarios for the origin of this structure: (1) a model specifically developed for application to this class of remnants, invoking a long evaporative timescale for the destruction of clouds engulfed by the SN blast wave (White & Long 1991) and (2) a model of remnant evolution in a homogeneous medium during the post-Sedov phase of development when radiative cooling at the shock front has become important. Because W44 is such a well-studied object, there is a wealth of information available on it. The distance is accurately known, and since there is an associated pulsar, we have an independent estimate of the age of the remnant. Our measurement of the mean temperature of the hot plasma in W44 from the X-ray observations, coupled with its age and size, provides the strongest constraints on the evolutionary state of the remnant.

Taking size and temperature as the fundamental observables, we find that the WL model predicts an age of 5600–7500 yr, which is incompatible with the characteristic age ($\sim 20{,}000$ yr) of the associated pulsar PSR $1853+0.1$. This is considerably greater than any discrepancy that could be explained though errors in calculating the distance to W44 or in the X-ray temperature measurements. It would require the pulsar in W44 to have been born as a slow rotator ($P_0 \gtrsim 200$ ms) or to have undergone an unusual spin-down history. The WL model also predicts an unusually low explosion energy of $\lesssim 0.2 \times 10^{51}$ ergs for the core-collapse SN that is believed to have formed W44 and PSR $1853+0.1$. These two observationally derived conclusions are the basis on which we reject the WL model as the explanation of this center-filled remnant in favor of the radiative shock phase model. However, we also wish to highlight the astrophysical implausibility of a major assumption of the WL model; i.e., that the ISM clouds engulfed by a SNR should survive being crushed by the blast wave and linger within the interior to be gently evaporated away on timescales that are many times the age of the remnant. We do not reject the WL model because we consider a cloudy ISM unlikely; rather, it is the *timescale* for the destruction of those clouds that is at issue.

Our alternative scenario for W44 places the remnant in the post-Sedov radiative phase of evolution. In this case, we find that a centrally peaked morphology and nearly uniform temperature profile can occur for models that are roughly 19,000–25,000 yr old, for reasonable explosion energies ($\sim 0.9 \times 10^{51}$ ergs) and ISM densities of 3–4 cm^{-3} (assumed uniform and homogeneous). These are not outrageously large values for the ambient density; rather, they are very similar to the ambient densities estimated around the SNRs N132D and N49 in the Large Magellanic Cloud (Hughes 1987; Vancura et al. 1992). These largish densities are attributed to the presence of nearby molecular clouds for the LMC SNRs (Banas et al. 1997). A similar explanation is likely for W44, since it too appears to be associated with molecular emission (Wootten 1977). Our model accounts naturally for the high-velocity shell of H I gas that surrounds the X-ray–emitting gas in W44. Finally, the radiative phase scenario is qualitatively consistent with the gross characteristics of the VLA radio image, with filamentary radio emission concentrated at the rim rather than in the remnant interior.

Additional research on W44 should be directed toward obtaining spatially resolved measurements of temperature and elemental abundances. These will be challenging measurements to make, since both the radiative phase model and the current data support the presence of only a modest radial variation in temperature. We are pursuing this issue further with the available *ASCA* data. It is also interesting to note that a more accurate estimate of the remnant's age may become available in the future. Recently, Frail et al. (1996) argued that the pulsar in W44 is moving to the south with a speed of approximately 375 km s^{-1}. Since the likely location of the SN explosion that gave rise to the pulsar is known (i.e., at the centers of the radio continuum, X-ray, and H I images of W44), measurement of the proper motion of PSR $1853+0.1$ (estimated to be of order 25 mas yr^{-1}) would provide a distance-independent determination of the age of the pulsar and the SNR. As we have shown in this article, such a definitive measurement would provide a crucial constraint on models for the evolutionary state of W44 and should be pursued.

We thank Fred Seward, Pat Slane, Olaf Vancura, and David Helfand for useful discussions and comments during the course of this project. Our research made use of data obtained from the High Energy Astrophysics Science Archive Research Center Online Service, provided by the NASA/Goddard Space Flight Center. K. P. S. acknowledges the hospitality of the High Energy Astrophysics Division of the Center for Astrophysics and thanks the Smithsonian Institution for funding his visit to the CfA. This research was supported in part by NASA under grants NAG 8-670, NAG 8-181, and NAG 8-287, and by Smithsonian Institution funds from the International Exchange Program and the Predoctoral Program through a fellowship awarded to I. M. H.

REFERENCES

Banas, K. R., Hughes, J. P., Bronfman, L., & Nyman, L.-Å. 1997, ApJ, 480, 607
Boyd, P. T., et al. 1995, ApJ, 448, 365
Christian, D. J., Swank, J. H., Szymkowiak, A. E., & White, N. E. 1992, Legacy, 1, 38
Cox, D. P. 1972, ApJ, 178, 159
Cui, W., & Cox, D. P. 1992, ApJ, 401, 206
Edge, D. O., Shakeshaft, J. R., McAdam, W. B., Baldwin, J. E., & Archer, S. 1959, MNRAS, 68, 37
Frail, D. A., Giacani, E. B., Goss, W. M., & Dubner, G. 1996, ApJ, 464, L165
Giacconi, R., et al. 1979, ApJ, 230, 540
Goss, W. M. 1968, ApJS, 15, 131
Goss, W. M., Caswell, J. L., & Robinson, B. J. 1971, A&A, 14, 481
Gronenschild, E. H. B. M., Mewe, R., Heise, J., Den Boggende, A. J. F., Schrijver, J., & Brinkman, A. C. 1978, A&A, 65, L9
Harrus, I., Hughes, J. P., & Helfand, D. J. 1996, ApJ, 464, L161
Hughes, J. P. 1987, ApJ, 314, 103
Hughes, J. P., & Helfand, D. J. 1985, ApJ, 291, 544
Hughes, J. P., Helfand, D. J., & Kahn, S. M. 1984, ApJ, 281, L25
Hughes, J. P., & Singh, K. P. 1994, ApJ, 422, 126
Hwang, U., Hughes, J. P., Canizares, C. R., & Markert, T. H. 1993, ApJ, 414, 219
Jones, L. R., Smith, A., & Angellini, L. 1993, MNRAS, 265, 631
Joyce, R. M., Becker, R. H., Birsa, F. B., Holt, S. S., & Noordzy, M. P. 1978, IEEE Trans. Nucl. Sci., 25, 453
Kaspi, V. M., Manchester, R. N., Siegman, B., Johnston, S., & Lyne, A. G. 1994, ApJ, 422, L83
Knapp, G. R., & Kerr, F. J. 1974, A&A, 33, 463
Koo, B.-C., & Heiles, C. 1995, ApJ, 442, 679
Kundu, M. R., & Velusamy, T. 1972, A&A, 20, 237
Long, K. S., Blair, W. P., Matsui, Y., & White, R. L. 1991, ApJ, 373, 567
Lyne, A. G., Pritchard, R. S., & Smith, F. G. 1993, MNRAS, 265, 1003
Lyne, A. G., Pritchard, R. S., Smith, F. G., & Camilo, F. 1996, Nature, 381, 497
Makino, F., et al. 1987, Astrophys. Lett. Commun., 25, 223 (Astro-C Team)
McKee, C. F., & Ostriker, J. P. 1977, ApJ, 218, 148
Mills, B. Y., Slee, O. B., & Hill, E. R. 1958, Australian J. Phys., 11, 360
Mohanty, D. K. 1983, in IAU Symp. 101, Supernova Remnants and Their X-Ray Emission, ed. J. Danziger & P. Gorenstein (Dordrecht: Reidel), 503
Morrison, R., & McCammon, D. 1983, ApJ, 270, 119
Pfeffermann, E., et al. 1986, Proc SPIE, 733, 519
Radhakrishnan, V., Goss, W. M., Murray, J. D., & Brooks, J. W. 1972, ApJS, 24, 49
Raymond, J. C., Cox, D. P., & Smith, B. W. 1976, ApJ, 204, 290
Raymond, J. C., & Smith, B. W. 1977, ApJS, 35, 419 (RS)
Rho, J. H., Petre, R., Schlegel, E. M., & Hester, J. J. 1994, ApJ, 430, 757
Scheuer, P. A. G. 1963, Observatory, 83, 56
Sedov, L. I. 1959, Similarity and Dimensional Methods in Mechanics (New York: Academic)
Seward, F. D., Schmidt, B., & Slane, P. O. 1995, ApJ, 453, 284
Shelton, R., & Cox, D. P. 1995, BAAS, 27, 3
Smith, A., Jones, L. R., Watson, M. G., Willingale, R., Wood, N., & Seward, F. D. 1985, MNRAS, 217, 99
Smith, R. C. 1996, Ph.D. thesis, Univ. Wisconsin at Madison
Snowden, S. L., McCammon, D., Burrows, D. N., & Mendenhall, J. A. 1994, ApJ, 424, 714
Taylor, J. H., Manchester, R. N., & Lyne, A. G. 1993, ApJS, 88, 529
Taylor, J. H., & Cordes, J. M. 1993, ApJ, 411, 674
Thielemann, F.-K., Nomoto, K., & Hashimoto, X. 1996, ApJ, 460, 408
Trümper, J. 1983, Adv. Space Res., 2(4), 241
Turner, M. J. L., et al. 1989, PASJ, 41, 345
Vancura, O., Blair, W. P., Long, K. S., & Raymond, J. C. 1992, ApJ, 394, 158
Vancura, O., Raymond, J. C., Dwek, E., Blair, W. P., Long, K. S., & Foster, S. 1994, ApJ, 431, 188
Westerhout, G. 1958, Bull. Astron. Inst. Netherlands, 14, 215
Wheeler, J. C. 1981, Rep. Progr. Phys., 44, 85
White, R. L., & Long, K. S. 1991, ApJ, 373, 543 (WL)
Wolszczan, A., Cordes, J. M., & Dewey, R. J. 1991, ApJ, 372, L99
Wootten, H. A. 1977, ApJ, 216, 440